Emergent higher-order interactions enable coexistence in phage-bacteria community dynamics

Raunak Dey[1,2,+], **Ashley R. Coenen**[2,+], **Natalie E. Solonenko**[3,4,+], **Marie N. Burris**[3], **Anna I. Mackey**[3,¶], **Julia Galasso**[3,†], **Christine L. Sun**[3,4], **David Demory**[5,#], **Daniel Muratore**[5,§], **Stephen J. Beckett**[5,6,7], **Matthew B. Sullivan**[3,4,8,9,*], and **Joshua S. Weitz**[1,2,5,6,7*]

[1]Department of Physics, University of Maryland, College Park, College Park, MD, USA
[2]School of Physics, Georgia Institute of Technology, Atlanta, GA, USA
[3]Department of Microbiology, The Ohio State University, Columbus, OH, USA
[4]Center of Microbiome Science, The Ohio State University, Columbus, OH, USA
[5]School of Biological Sciences, Georgia Institute of Technology, Atlanta, GA, USA
[6]Department of Biology, University of Maryland, College Park, College Park, MD, USA
[7]University of Maryland Institute for Health Computing, North Bethesda, MD, USA
[8]Department of Civil, Environmental and Geodetic Engineering, The Ohio State University, Columbus, OH, USA
[9]NSF EMERGE Biology Integration Institute, Ohio State University, Columbus, OH, USA
[¶]present: Molecular Genetics and Microbiology, Duke University, Durham, NC, USA
[†]present: Department of Neurology, Icahn School of Medicine at Mount Sinai, New York City, NY, USA
[#]present: Sorbonne Université, CNRS, USR 3579, Laboratoire de Biodiversité et Biotechnologies Microbiennes (LBBM), Observatoire Océanologique, Banyuls-sur-Mer, France
[§]Santa Fe Institute, Santa Fe, NM, USA
[*]Corresponding authors: sullivan.948@osu.edu, jsweitz@umd.edu
[+]these authors contributed equally to this work

ABSTRACT

Diverse phage-bacteria communities coexist at high densities in environmental, agricultural, and human-associated microbiomes. Phage-bacteria coexistence is often attributed to coevolutionary processes mediated by complex, pairwise infection networks. Here, using *in vitro* experiments and mathematical models, we explore how higher-order interactions function as a complementary, ecological feedback mechanism to stabilize phage-bacteria communities. To do so, we examine an environmentally-derived, synthetic phage-bacteria community comprised of five marine heterotrophic bacteria (*Cellulophaga baltica* and *Pseudoalteromonas* strains) and five associated phage. We used Bayesian inference to reconstruct free phage production in one-step growth experiments and then forecasted pairwise phage-bacteria dynamics over multiple infection cycles. In contrast to model predictions of rapid bacterial population collapse, each bacterial strain persisted, consistent with density-dependent stabilization mechanisms at high virus densities. We then extended models into a community context and found an additional stabilization mechanism: life history traits differ in community vs. pairwise contexts. Follow-up experiments confirm that lysis is inhibited at relatively high viral densities and phage traits (including burst size) can shift when infecting single vs. multiple strains. More broadly, these findings suggest that complex community coexistence of phage and bacteria may be more common than anticipated when including feedback mechanisms outside of regimes of fitted pairwise models that do not reflect the full scope of ecologically relevant contexts.

1 Main

Bacteriophage ('phage') shape bacterial population dynamics in human-associated, built environments, and environmental microbiomes[1–11]. Phage infections of bacteria are highly specific, such that realized interactions between phage and bacteria can be represented as complex, sparse networks[12]. At microevolutionary scales, phage-bacteria coevolve generating interaction networks with nested structures such that phage span a range of generalists to specialists and bacteria span a range of permissive to resistant[7]. However, when greater diversity of phage and bacteria are considered, then phage-bacteria interaction networks exhibit modularity in which a subset of phage preferentially infect restricted subsets of bacteria[8]. Phage-bacteria interactions can also exhibit multi-scale structure both in large-scale marine surveys [8,10] and within experimental coevolutionary studies beginning with joint inoculation of a single phage and bacterial type[13]. It remains an open challenge to connect niche differences due to pairwise interaction network structure with ecological feedback mechanisms that enable the emergence and maintenance of complex phage-bacteria communities.

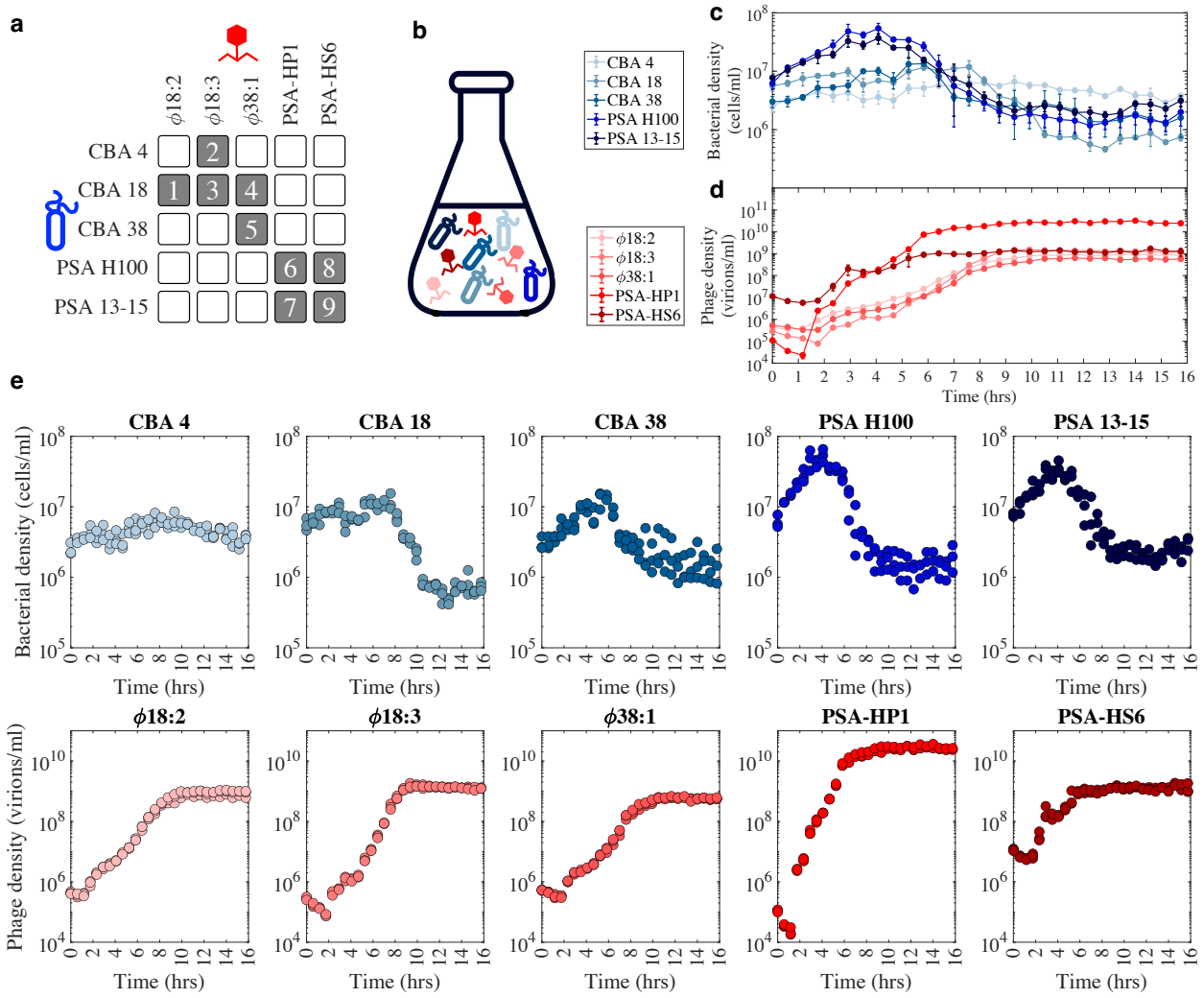

Figure 1. Community experimental data. (a) Adsorption assay experiments reveal an infection matrix with nine out of twenty-five possible infections occur among the strains, each numbered in a shaded gray box. Empty white boxes denote the absence of evidence for infection of the phage strain (in the columns) with the bacterial strain (in the rows). **(b)** Cartoon schematic of the five phage and five bacterial strains coexisting together in the same flask. **(c–d)** The experimentally recorded mean bacteria and phage population time series measured via qPCR are plotted along with their respective standard deviations (see Methods). **(e)** Separate panels depict measurements from three experimental replicates for each of the 5 host and 5 phage strains in the community experiment shown in (b) and averaged in (c) and (d).

Decomposing communities into pairwise interactions is typically a first approach to understanding how complex interaction networks affect population and community dynamics. To do so also requires measurements of bacterial and viral-associated life history traits. Baseline interactions between phage and bacteria can be characterized in a pairwise fashion given cultured isolates[7,13,14]. These culture-based approaches allow for quantitative measurements of ecologically relevant life history traits such as bacterial growth rates and viral adsorption rates, latent periods, and burst sizes[15–17]. Scaling up pairwise interactions to community interactions has been used to predict coarse-grained patterns and processes of community assemblages[18–21]. But pairwise interactions often fail to capture the emergent stability and co-existence of communities that arise from factors such as higher-order interactions[22–25], context dependent emergent effects[26–28], temporal partitioning[29], density-dependent feedback[30], and environmental feedback[31]. Pairwise models typically assume static interactions, ignoring the effects of changing environmental conditions and feedback loops[32–34]. These mechanisms may also be relevant in reconciling gaps between predicted community outcomes derived from pairwise interactions between phage and bacteria.

In this paper, we combine ecological theory, models, and direct experimental measurements to assess the limits to

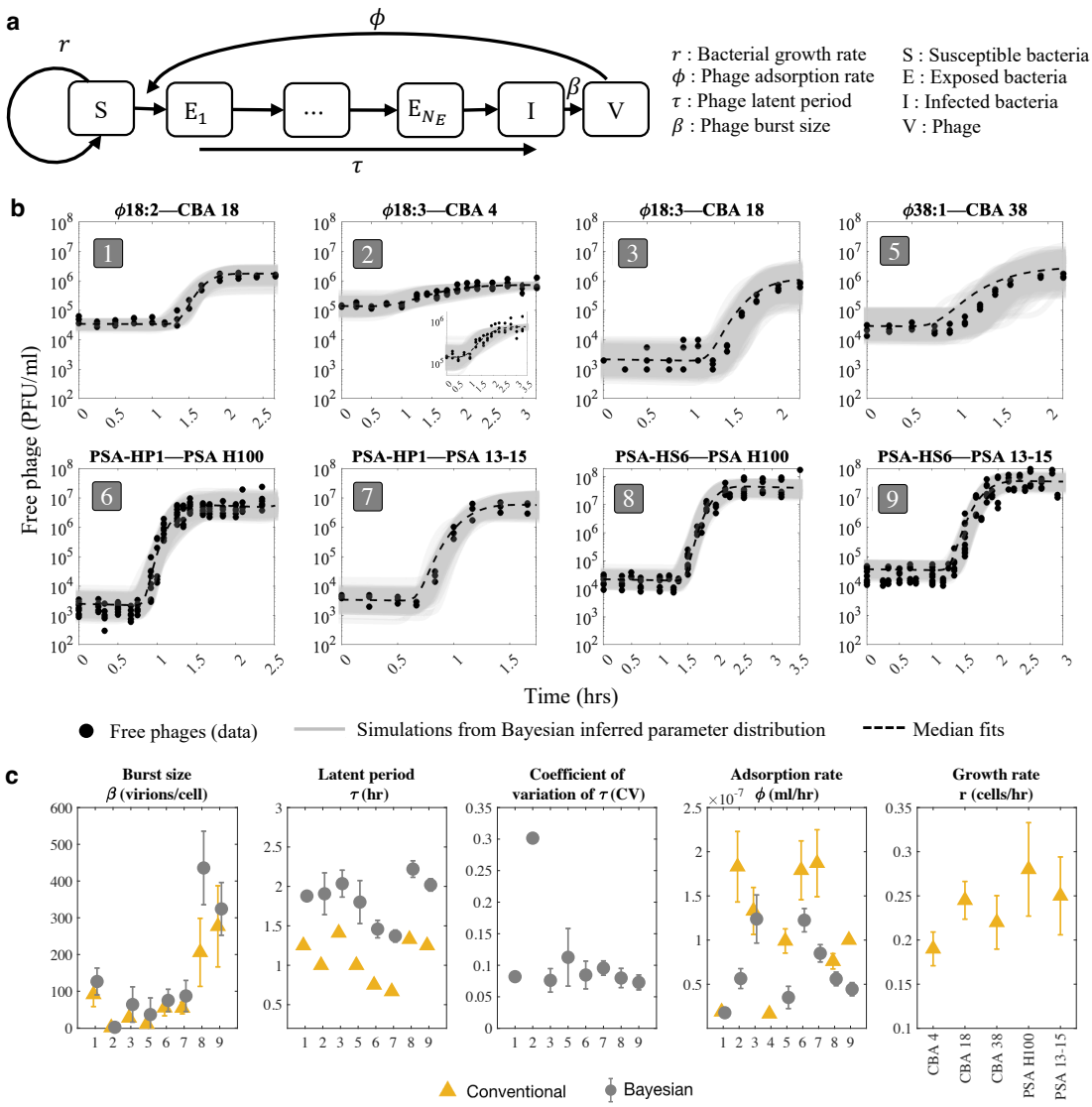

Figure 2. Pairwise interactions between phage and bacteria. (a) Pairwise phage-bacteria dynamics fit with a nonlinear ODE model (described in Supplementary Information S1.1) with a variable number of compartmental stages of infection N_E (Supplementary Information Fig. S1), parameterized by the specific phage–bacteria pairwise life history traits: r, ϕ, τ, β. **(b)** Free phage density measured through one-step growth curves (black dots) for eight out of nine interacting phage–bacteria pairs. Using the model in (a), the pairwise life history parameters β, τ, and ϕ are inferred by a Bayesian algorithm. The Bayesian fits are shown in gray lines along with 95% credible interval shaded for each of them. **(c)** The conventionally inferred life history traits from single-strain experiments (yellow triangles) such as one-step growth curves, pairwise adsorption assays, and bacterial growth doubling time experiments are compared to Bayesian inferred life history traits (gray circles) from one-step growth curves; standard deviations shown as error bars. The interactions are labeled in Fig. 1a. The coefficient of variation for the latent period distribution (related to the inferred number of compartments N_E as $\frac{1}{\sqrt{N_E+1}}$) is also inferred for each pair. Full details on the fitting procedure are provided in Supplementary Information Fig. S6.

predictability of dynamics within a community of intermediate complexity given five bacterial strains from two different species of marine heterotrophic bacteria (*Cellulophaga baltica* and *Pseudoalteromonas* strains) and five virulent bacteriophage[35–37]. All five bacterial strains and five phage strains were originally isolated from similar conditions in marine waters and coexist in a synthetic community in laboratory conditions. Beginning with pairwise interactions, we used a nonlinear population model to infer life history traits from time series measurements of phage and bacteria abundance. The nonlinear model predicts rapid bacterial collapse within a few lytic cycles – in direct contrast to experimental evidence. Instead, we find that higher-order interactions and density-dependent feedback can enable phage-bacteria coexistence in complex communities that

was not anticipated from short-term, pairwise experiments in regimes where viral densities are relatively low. As we show, this iterative use of models and experiments reveals novel mechanisms that may enable coexistence of complex phage and bacterial communities – and provides a caution for extrapolating community-scale outcomes from a narrower scope of conditions than expected in ecologically relevant contexts.

2 Results

Multiple bacteria and their associated phage coexist in the same community

We sought to assess whether a complex community of five bacteria that includes three *Cellulophaga baltica* (CBA) and two *Pseudoalteromonas* (PSA) isolated from similar environmental conditions could coexist at timescales spanning multiple life cycles when mixed with five associated virulent phage (see Methods in Sec. 4 for strain details). To do so, we first identified the host range of each of the five phage – identifying nine positive interactions among twenty-five combinations. The resulting infection matrix is modular such that the phage strains associated with either CBA or PSA do not cross-infect the other species (Fig. 1a). Next, we combined all five bacteria at the same initial densities and their five associated phage strains at a fixed multiplicity of infection (MOI) of 0.1 (Fig. 1b). We sampled the *in vitro* community dynamics through triplicate experiments, recording cell and virion densities through intracellular quantitative Polymerase Chain Reaction (qPCR-INT) and extracellular quantitative Polymerase Chain Reaction (qPCR-EXT), respectively, every 35 minutes for 15.75 hrs, resulting in 28 time points for each flask (see Methods for further details on culture conditions and sampling methods). All 5 bacteria and 5 phage strains coexist for the duration of the experiment (means and standard deviations shown in Fig. 1c,d and replicates shown in Fig. 1e). The high-resolution sampling of the phage–bacteria community also revealed subtle transient dynamics. Initially, phage populations decline given adsorption to cells even as cell populations increase given the relatively low initial impact of viral lysis. Subsequently, viral populations increase via infection and lysis (Fig. 1d-bottom row), leading to bacterial density declines ∼4–8 hrs after inoculation, albeit stabilizing to levels between 10^5 cells/ml to 10^7 cells/ml at the conclusion of the experiment. Similarly, phage populations stabilize between 10^9 virions/ml to 10^{11} virions/ml, coexisting with, rather than eliminating, the bacterial populations.

Inferring pairwise phage–bacteria dynamics and traits

In order to reconcile the finding of elevated phage densities with community coexistence, we set out to quantify bacterial growth rates as well as intracellular and extracellular phage life history traits and then embed those into pairwise population models (Fig. 2a). We measured the growth rate r through doubling time experiments, finding that CBA strains divided every 4.2 – 5.8 hrs and PSA strains divided every 3.6 – 3.8 hrs (Fig. 2c). Next, we estimated the adsorption rates of each of the five phage to their respective hosts using adsorption assays with ranges between $\sim 2\times10^{-8}$–2×10^{-7} ml/hr (Fig. 2c). New phage began to appear 0.5 hrs to 1.5 hrs later. For each interacting phage–bacteria pair, we used a Bayesian MCMC approach to fit a Susceptible-Exposed-Infected-Virus (SEIV) infection population model to one-step growth curves (Supplementary Information Fig. S1 and Methods S1.1, with prior distributions informed from conventional trait estimates). One-step growth experiments were not obtained for the interaction of phage ϕ38:1 on CBA 18 due to methodical challenges associated with inefficient infections for this pair[38]. The SEIV model recapitulated phage production dynamics in one-step growth curves (Fig. 2b). Fitted models provide posterior estimates of life history traits including the adsorption rate ϕ, mean latent period τ, coefficient of variation of the latent period $CV(\tau)$, and burst size β. We compared Bayesian inferences of traits with 'conventional' methods[15] that utilize the time of first appearance of viruses and viral plateau to infer traits in Fig. 2c (as summarized in Supplementary Information Table S3). The conventional approach to inferring the mean latent period from one-step growth curves underestimates the mean latent period by neglecting variability in latent period outcomes among infected cells in a population[17]. We estimate the coefficient of variation of the latent period to be ≈ 0.1 for most strains. As is shown in Fig. 2b, the nonlinear SEIV model of phage-bacteria interactions with inferred life history traits can recapitulate virus production dynamics over a single lytic period.

Dynamics of pairwise infections over multiple infection cycles

We reinitiated all 8 viable, pairwise infection experiments focusing on phage-bacteria pairs for which we have robust parameter estimates (as described in the prior section). Throughout, we measured host densities via qPCR at $t = 0$ and $t = 15.75$ hrs (details in Sec. 4), consistent with time scales in the community experiment. As a baseline, we measured initial and final host densities in uninfected control populations. The ratio of final to initial host density in control (phage-free) populations varied from 10 to nearly 100, consistent with host proliferation in the absence of phage. We hypothesized that addition of phage would lead to the collapse of bacterial populations. In fact, host populations persisted in all cases to the end of the experiment in the presence of phage. The ratio of final to initial host density in infected populations was lower than in uninfected controls and varied from approximately 10^{-1} to 10. In all cases, the ratio of final to initial host density in infected populations was lower than that in control populations (see Fig. 3a - contrast black circles with open circles).

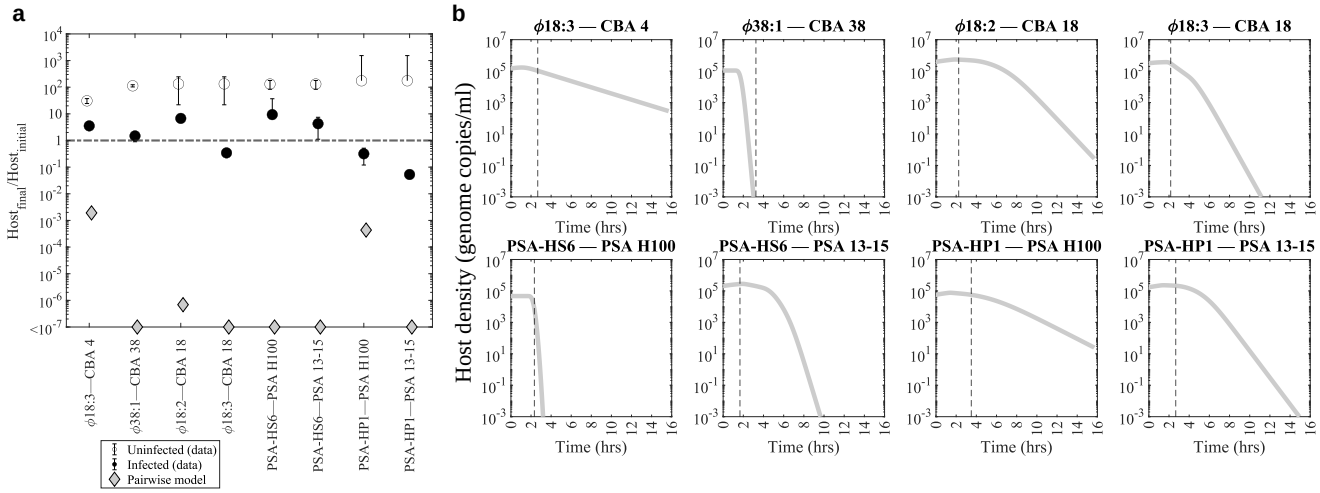

Figure 3. Host densities from pairwise infection experiments over multiple life cycles. Pairwise model is parametrized with the one-step parameters (Fig. 2) and experimentally recorded initial densities for 8 infection pairs. **(a)** Each experiment is performed for 15.75 hrs, representing multiple life cycles. Ratios of qPCR measured final (at 15.75 hrs) to initial (at 0 hrs) host densities for the 8 pairs of infection (infected in solid circles, control in white circles) and pairwise model (gray diamonds). Constant abundance is represented by the dashed line. **(b)** Pairwise model predicted dynamics of the infected hosts plotted for experimental timescales. The vertical dashed line shows the time up to which the corresponding one-step experiment was performed in each case.

To explore dynamics of pairwise infections over multiple infection cycles, we simulated pairwise SEIV models for each pair. We initialized each of the 8 pairwise models at a host density of $\approx 10^5$ ml^{-1}, consistent with measured host densities. Life history traits were set to those inferred through single-cycle pairwise experiments as shown in the prior section. Despite fitting one-step growth curves, the pairwise SEIV models predict population crashes within 16 hrs for 5 out of the 8 host phage pairs (see Fig. 3b) and predict substantial host population declines of at least a factor of 10^2 in all cases. In contrast, we found that 5 out of 8 experiments with infected populations exhibited increased host densities and never exhibited host population declines greater than a factor of 10^2. This finding implies that host growth remains largely in balance and potentially exceeds viral lysis in the majority of pairs, in strong contrast to simulated dynamics in models that inferred apparently efficient lysis within one-step growth experiments. This discrepancy suggests the presence of additional stabilizing mechanisms for these environmentally derived strains that could mediate coexistence as observed in community experiments.

Scaling-up pairwise infection model and traits to the community level

We extended the pairwise SEIV model to a community context by incorporating cross-infections as obtained through adsorption assay experiments (Fig. 1a). In the community model each susceptible bacteria population, i, with density S_i can be infected by each of its associated phage, j, with density V_j. For each of the nine pairs, we account for the classes of exposed compartments E_{ij} including latent period heterogeneity. We specifically excluded the potential for multiple infections of a single cell, either by the same or different phage. The community SEIV model is parameterized by nine pairs of burst sizes, latent periods, and adsorption rates and five bacterial growth rates (see Fig. 4 and Supplementary Section S1.2 for details).

We simulated the community SEIV model using the pairwise Bayesian median posterior estimates of the viral burst sizes, adsorption rates, average latent periods and their variability for the eight inferred interactions, and bacterial growth rates (Fig. 2c and Supplementary Information Table S3). As noted, one-step phage growth parameters could not be inferred for the infection of ϕ38:1 on CBA 18. Instead, we used a range of parameter values derived from the literature[38]. The community SEIV model parameterized by pairwise-fitted infection traits failed to capture the observed community dynamics. As in the pairwise simulations over multiple infection cycles (Fig. 3b), the community SEIV model predicts that all bacterial populations should decrease rapidly given the explosive growth of phage populations (Fig. 5a). Even when accounting for variability in life history traits, the models predict decreases exceeding two orders of magnitude within 10 hrs post-exposure to viruses. This bacterial population collapse (not observed in experiments and akin to that shown in pairwise SEIV models) arises via rapid increases and then stabilization of viral populations.

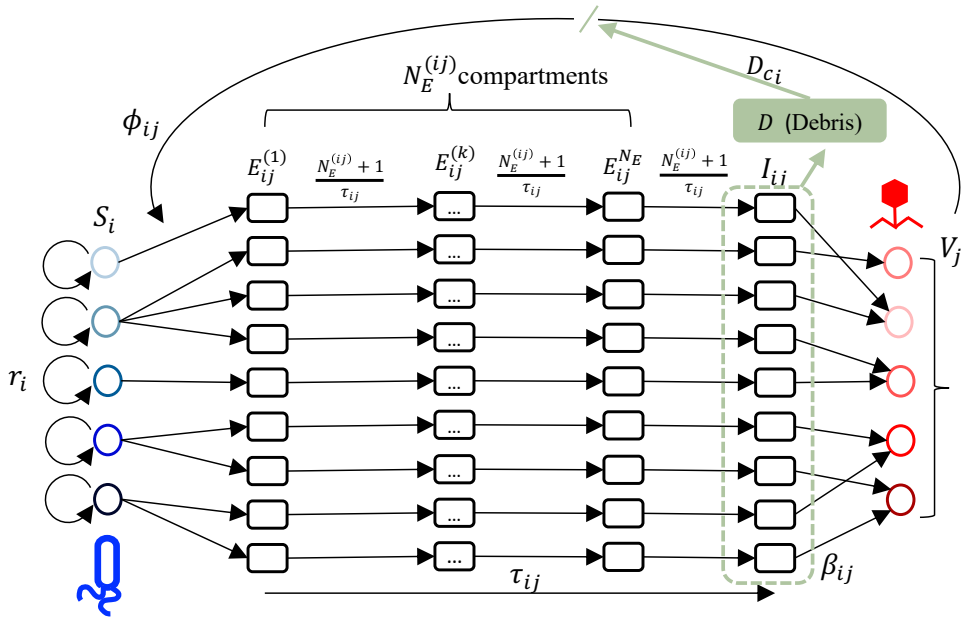

Figure 4. SEIV and SEIVD based scaled-up community model. Using the infection matrix in Fig. 2(b) the model is scaled up to include the 9 interactions between 5 bacterial and 5 phage strains and respective number of exposed classes $N_E^{(ij)}$ for each interaction. S_i, E_{ij} and I_{ij} are susceptible, exposed, and infected stages in the sequential infection for each bacteria i by phage j. This SEIV community model is parameterized by the phage infection traits of the constituent pairs of the community, such as, latent periods (τ_{ij}), adsorption rates (ϕ_{ij}), burst sizes (β_{ij}) and bacterial growth rates (r_i). For the SEIVD model, we include a state variable D, which represents the dead cell density (green box) that can inhibit new infections, given a critical debris concentration D_{c_i}. See main text and Supplementary Information S1.2 and S1.3 for the full description of the SEIV and SEIVD models, respectively.

Integrating higher-order interaction terms into the community model enables coexistence

We hypothesize that higher-order interaction terms inhibit new infections when viruses reach high densities and enable multi-strain coexistence. We explore two potential (and not mutually exclusive) mechanisms: (i) life history traits change in the community context; (ii) density-dependent feedback limits infections in the presence of significant lysis.

First, we refit the community SEIV model to the first 6.4 hrs of community dynamics by optimizing the fitted dynamics for the infection traits of all strains using Bayesian MCMC inference (see Supplementary Information Section S1.5.3). The re-fit community SEIV model quantitatively captured the population dynamics of all the phage strains for the entire 15.75 hr experiment (Fig. 5b-bottom) while only capturing bacterial dynamics for the first $\sim$ 6 hrs (Fig. 5b-top). The SEIV model fails to quantitatively fit the whole duration of the community dynamics, as it lacks a density-dependent feedback mechanism to prevent later-stage bacterial mortality (Supplementary Information Fig. S8 and Section S1.5.4). Nevertheless, the community SEIV model fits on the shorter timescale suggest that viral life history traits can differ between pairwise and community contexts (Supplementary Information Tab. S4).

Second, we extended the community SEIV model to assess the impact of a negative feedback mechanism in which bacterial lysis inhibits new infections, e.g., potentially due to inhibitory effects of cellular debris on viral adsorption and lysis. This new SEIVD model (where 'D' represents debris, see Fig. 4) includes a negative feedback loop in which the strength of infection inhibition is given by a Hill function given a critical strain-specific concentration, D_{c_i} (Supplementary Information Fig. S2). Complete details of the community SEIVD model are described in Supplementary Information S1.3. We evaluated the SEIVD model by performing MCMC-based Bayesian inference on the triplicate population time series data to estimate the joint posterior distribution of the phage–bacteria life history traits and D_{c_i} values. Unlike either the scaled-up pairwise model or the re-fit SEIV community model, this SEIVD community model can quantitatively fit both the experimentally recorded bacterial and phage time series data (Fig. 5c). We observed the phage dynamics include both initial decreases reflecting virion adsorption and subsequent recovery beyond initial viral densities while eventually stabilizing at levels consistent with observations. Likewise, the ensemble of bacterial density dynamics includes stabilization in all cases, as well as the potential

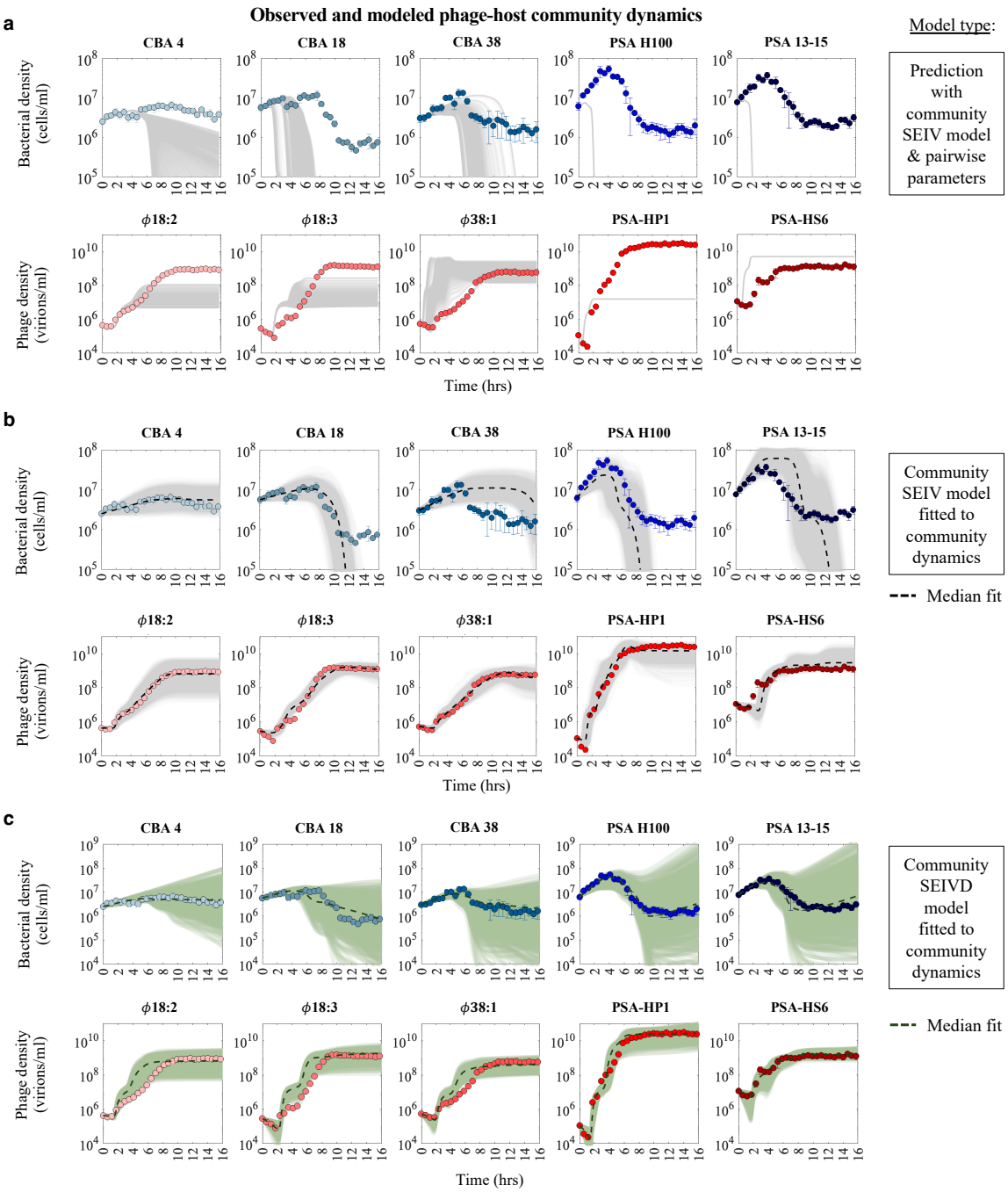

Figure 5. Comparison of observed versus simulated phage–bacteria population dynamics. The mean and standard deviations of the population density time series for all the five bacterial hosts and five phage obtained from triplicate experiments are shown (circles), with their respective standard deviations. **(a)** The life history traits inferred from single strain experiments and one-step growth curves in Fig. 2 are directly used to parameterize the scaled-up community model, where uncertainty in model outcome (gray lines) is associated with uncertainty regarding the burst size and latent period of ϕ38:1 on CBA 18 derived from literature (parameters summarized in Supplementary Information Table S3). With MCMC-based Bayesian inference, the scaled-up SEIV model fitted to the first 6.4 hours of the experiment successfully captures the initial part of the dynamics and predicts the later phage densities accurately while predicting selective bacterial strain elimination. The SEIV model is unable to fit bacterial dynamics for the whole duration (see Supplementary Information Fig S8). The fits from 95% credible intervals of the inferred parameter posteriors are plotted in gray, and median fits are shown with dashed lines. **(c)** The SEIVD model is used to infer community-level life history traits. Simulations from 95% Bayesian credible intervals of the posterior distribution are plotted in green and median fits in dashed lines. Priors are detailed in Supplementary Information Table S5 and posterior distributions in Supplementary Information Fig. S9. Additional information on fits is available in Supplementary Information Fig. S10 for the MCMC chains and Supplementary Information Fig. S11-S12 for the MCMC convergence statistics.

for bacterial population rebounds.

Experimentally testing putative higher-order interaction mechanisms

We set out to test both of the putative mechanisms involving higher-order interactions that could shape community-scale coexistence in the SEIVD model. First, we set out to test whether life history traits shift in a community context. Notably, the SEIVD community model predicted significant shifts in burst sizes, e.g., the community estimated burst size of PSA-HP1 is larger and that of PSA-HS6 is smaller compared to values inferred in pairwise experiments. To test these unexpected shifts, we performed one-step growth experiments of the PSA strains with all hosts combined (1 phage with the 5 host subcommunity). We found that in the subcommunity of PSA hosts the burst size of PSA-HP1 increases, whereas the burst size of PSA-HS6 decreases relative to the pairwise case, consistent with model-inferred predictions (see Supplementary Information S2.3, Fig. S5 and t-test results in Table S8). Next, in order to test for density-dependent inhibition of infection, we added bacteria-filtered and phage-inactivated spent media from 12 hrs of the community experiment to fresh pairwise infections for all 9 phage-bacteria infection pairs. In each case, we contrasted dynamics with that including the host alone and the phage-bacteria infection pair without community spent media. Host densities remained elevated for all strains in the phage-free control. For 3 CBA infections and 1 PSA infection, the host density falls below the limit of detection in the infection-only control (without community lysate). In contrast, the host density persists when community spent media is added along with the phage (Supplementary Information Fig. S3), consistent with a negative feedback loop on infection and lysis.

3 Discussion

In this work, we explored mechanisms of coexistence within a synthetic marine phage–bacteria community. In contrast to model predictions derived from short-term pairwise phage-bacteria experiments, we found that individual phage-bacteria pairs and complex multi-strain communities can coexist over multiple infection cycles. Through a process of iterative model-data integration, we hypothesized that higher-order interactions stabilize community dynamics. These interactions include context-dependent shifts in life history traits and infection inhibition at relatively high viral densities. By incorporating both types of higher-order interaction mechanisms, we quantitatively recapitulate community time series data and the coexistence of all 5 heterotrophic bacteria and 5 associated phage over a 15.75 hr time series experiment (far longer than the typical infection cycles of 1-2 hrs). In doing so, we also experimentally validated the model-inferred higher-order interaction mechanisms: life history traits exhibit directional shifts in community vs. pairwise experiments and phage lysates diminish the intensity of infection-induced lysis.

Central to our analysis was the development of a nonlinear population model that incorporated the combined effects of infection inhibition and emergent shifts in phage–bacteria life history traits. Higher-order interactions may be powerful drivers of community coexistence[19,39,40]. Previous studies have indicated that higher-order interactions affect short-term transient dynamics and long-term emergent stability of microbial communities[24,25,41–45]. More generally, higher-order interactions can also impact life history traits[26,46]. Life history traits can also depend on context, including host cell abundance or diversity[5,32,47], co-infection[48], and/or bacterial resistance[49]. Phage latent period may decrease in response to lower resources[50], and phage growth can be affected by bacterial growth rate[51]. The lower adsorption rates in the community might be a result of lower effective contact rates, despite higher initial concentrations, given the presence of multiple species as well as due to the accumulation of cellular debris[52]. This finding provides some caution of extrapolating from pairwise interactions: in some cases ecological models may have been fit to dynamics that do not fully represent feedback across biologically relevant regimes.

Our modeling and inference framework comes with caveats. A salient feature of our ecological models is the explicit integration of the variability in latent period observed in prior phage host systems[53–55] modeled via multi-compartment stages of infection progression[17,56]. For simplicity, we assumed that the variability in this latent period is the same for all pairwise interactions in the community SEIVD model. In reality, we expect variability to be heterogeneous. Another key assumption is that bacterial growth rates, latent periods and burst sizes are constant over time. However, net bacterial growth rates can be reduced via competition for resources and, in other contexts, increased through cross-feeding[57,58]. Moreover, burst sizes can change in response to variation in community abundances[59,60]. Further, we have assumed that each bacterial strain is infected by one virus at a time. Previous studies have shown that the outcomes of infection may differ depending on the multiplicity of infection, either in superinfection scenarios when multiple phage strains infect the same bacterial species or in cross-infection scenarios when distinct phage infect the same bacteria[61–63], but with different efficiencies. Future models would benefit from considering the impact of additional interactions and the potential to include time-varying or plastic traits. Such efforts will broaden our understanding of phage-bacteria dynamics across scales.

In summary, our work suggests that pairwise interactions inform but do not wholly determine community-level interactions. We find that higher-order interactions matter and that assuming rapid pairwise lysis does not necessarily explain phage–bacteria community dynamics and coexistence. The community models and inference framework developed here may be of service in exploring the generality of these feedback mechanisms in environmental, agricultural, and human-associated microbiomes[64–66].

In doing so, our work also presents a caution: scaling up results from pairwise interaction outcomes to community dynamics will almost certainly require accounting for higher-order interactions. Identifying the relevance of higher-order interactions is likely to improve the predictive capacity of community-scale models as well as provide insights into cross-system principles that enable the coexistence of diverse populations of virus and bacteria.

4 Methods

Strains and growth conditions

Five bacterial strains were used: *Cellulophaga baltica* strains NN016038, #4 (1), and #18 (2) were isolated from the Baltic Sea in 1994 (NN016038, hereafter CBA 38) and (3) in 2000 (#4 and #18, hereafter CBA 4 and CBA 18[67]); while *Pseudoalteromonas* sp.H100 (4) and 13-15 (5) were isolated from the North Sea in 1990 (hereafter PSA H100 and PSA 13-15[68]). Five bacteriophages were used: 1) ϕ38:1, a podovirus isolated from the Baltic Sea in 2005 on CBA 38, 2) ϕ18:2, a siphovirus isolated from the Baltic Sea in 2000 on CBA 18, 3) ϕ18:3, a podovirus isolated from the Baltic Sea in 2005 on CBA 18[67], 4) PSA-HP1, a podovirus isolated from the North Sea in 1990 on PSA H100, and 5) PSA-HS6, a siphovirus isolated from the North Sea in 1990 on PSA 11-68 (strain not included in this study[69]). Bacteria were grown on *Pseudoalteromonas-Cellulophaga* (PC) plates (20.5g Sigma Sea Salts, 1.5g peptone, 1.5g proteose peptone, 0.6g yeast extract, 13g agar/L) at room temperature (RT). Single colonies were inoculated and grown stationary at RT overnight in PC liquid growth medium (20.5g Sigma Sea Salts, 0.75g peptone, 0.5g yeast extract, 0.25g proteose peptone, 0.25g casamino acids, 1.5ml glycerol/L). Phage strains were stored in phage buffer (20.5g Sigma Sea Salts/L) and plaque forming units (PFUs) enumerated using the agar overlay method (Sambrook and Russell 2001) with 3.5ml molten soft agar (20.5g Sigma Sea Salts and 6g low melting point agarose/L) and 300μl overnight bacterial culture per plate.

Community experiment

The community experiment was performed in triplicate with all five bacterial strains and all five phage strains together. Bacterial strains were inoculated and transferred individually; transfer cultures were pelleted at 4,000g for 10 minutes and 4×10^8 cells of each strain (2×10^9 total cells) were added to 200ml PC growth medium in each of 6x 2L flasks. Phage strains were then added at an MOI of 0.1 (4×10^7 each phage, 2×10^8 total phage) to three flasks while three contained no phage, and samples were taken every 35 minutes for 15 hours 45 minutes. At each time point, we sampled for OD_{600}, CFUs, intracellular qPCR quantification (qINT), and extracellular qPCR quantification (qEXT).

Primers for qPCR were designed to amplify 75-150bp portions of each bacterial strain or phage, with negligible amplification from other members of the community. The primers were designed using the complete genomes of each bacterial strain or phage. All bacterial and phage genomes are sequenced and publicly available but 2 of the bacterial genomes were not complete (*Cellulophaga baltica* 4 and *Pseudoalteromonas* sp. H100) and existed in genome fragments. To rectify this, we applied long-read sequencing to resequence and complete those two genomes. In addition, we also resequenced *Pseudoalteromonas* sp. 13-15 since primer design was difficult for the two *Pseudoalteromonas* bacterial strains as they are 99.9% identical genomically.

Primer pairs were tested for efficiency and mis-priming, and we used only primers with >85% efficiency and <10 copies/μl amplification from other community members. DNA was extracted from qINT samples using the DNeasy Blood and Tissue kit (Qiagen) following the manufacturer's instructions; qEXT samples were used as-is. qPCR was performed on an Eco Real-Time PCR System (Illumina) with PerfeCTa SYBR Green FastMix Reaction Mix (QuantaBio) in 13μl reactions. Per reaction, we used 6.5μl PerfeCTa master mix, 0.39μl 10mM forward primer, 0.39μl 10mM reverse primer (Supplementary Information Tab. S7), 4.72μl nuclease-free water, and 1μl template. For qINT samples, extracted DNA was used as template, and for qEXT the 0.2μm filtrate was used. Reactions were performed in technical duplicates with a standard curve consisting of 5x 10-fold dilution series of known concentration of the target strain or phage, used to calculate target sequence copies/μl. Cycling conditions were as follows: polymerase activation for 5 minutes at 95°C; 40 cycles of 20 secs at 95°C, 10 secs at primer annealing temperature (Supplementary Information Tab. S7), and 20 sec at 72°C, and a 55°C – 95°C melt curve.

Single bacteria and pairwise phage–bacteria experiments

Bacterial growth curves to determine doubling times were performed in triplicate in PC growth medium on cultures transferred 1:20 from overnight cultures into new media, grown stationary at RT. A regression of OD_{600} and colony forming units (CFUs) was constructed using exponential phase time points to estimate cell density from OD readings.

Adsorption of phage to bacterial strains was characterized in triplicate by combining one phage with one bacterial strain and enumerating free (0.2μm filtered to remove bacteria) and total phage over time. Pairs with a known interaction were combined at a multiplicity of infection (MOI) of 0.1 (10^7 phage and 10^8 cells/ml) and total and free phage PFUs were enumerated every 3-5 minutes for 24-25 minutes to calculate the adsorption constant. Pairs with no known interaction were combined at an MOI of 3 (3×10^8 phage and 10^8 cells/ml), and total and free phage PFUs were enumerated at time intervals for 3 hours to

examine evidence in support of a statistically significant decrease in free phage. All infections were performed with strains in mid-exponential phase.

One-step growth curves were performed in triplicate to determine phage burst sizes and latent periods. Each phage–bacteria pair was combined at an MOI of 0.1 (10^7 phage/ml and 10^8 cells/ml) and incubated for 15 minutes to allow phage to adsorb to cells. The infection was then diluted 1:100 in PC growth medium to reduce the chances of new adsorptions. Total and free phage PFUs were enumerated at regular intervals for 2-4 hours. The conventional latent period was determined as the length of time before a significant increase in phage concentration. The average burst size $\langle\beta\rangle = \frac{\langle V_2\rangle - \langle V_1\rangle}{\langle T_1\rangle - \langle V_1\rangle}$ where V is the free phage density before (V_1) and after (V_2) the burst event, and T_1 is the total phage density before the burst event. The averages $\langle\cdot\rangle$ are taken over multiple time points and experiment replicates. All infections were performed with strains in mid-exponential phase.

Pairwise experiment for multiple infection cycles

Each bacterial strain was inoculated, transferred, and pelleted as previously described. All pairwise phage-host interactions were tested in triplicate, with triplicate uninfected controls for each strain. Each strain was diluted to 2×10^7 CFU/ml in PC media, and a single phage was added at an MOI of 0.1. From this infection, we immediately sampled to quantify total and free phage as previously described, and for intracellular (qINT) and extracellular (qEXT) qPCR. For qPCR, 1ml was pelleted at 10,000g for 5 minutes at 4°C. The supernatant was 0.2μm filtered to remove any unpelleted bacteria and stored at 4°C for qEXT analysis and the pellet was flash frozen in liquid nitrogen and stored at -80°C for qINT analysis. We also aliquoted the infections into wells of a 96-well plate and read OD_{600} at 35-minute intervals for 15.75 hrs. At the end of this time, we repeated total phage, free phage, qEXT, and qINT sampling from the infection wells, pelleting 150μl instead of 1ml. DNA was extracted from qINT pellets using the DNeasy Blood and Tissue kit (Qiagen), following the manufacturer's instructions for Gram-negative bacteria. qPCR was performed to quantify intracellular and extracellular phage and bacterial DNA as previously described.

Modeling

We developed a coupled system of nonlinear ordinary differential equations (ODEs) to represent the dynamics of susceptible (S), exposed (E) and infected (I) bacterial cells and viruses (V). This SEIV model is parameterized by the viral latent period (τ), burst size (β), adsorption rate (ϕ), and bacterial growth rates (r). We utilized a non-stiff ODE solver with an adaptive time step[70] and fixed constraints. Variation in the latent period distribution is incorporated through a compartmental model of E classes[17] which generates Erlang distributed latent periods[71]. Supplementary Information Section S1.1 contains a full model description. The community SEIV model is scaled up to include interaction specific traits of all 9 phage-bacteria pairs. The SEIVD model also includes a state variable representing cellular debris (D), a proxy for the cumulative number of lysed cells. We assume debris inhibits infection via a Hill function given by $\frac{1}{1+(D/D_{c_i})^2}$ given the half-saturation constant D_{c_i}. Supplementary Information Section S1.2 & S1.3 provides details on the community SEIV and SEIVD models, respectively.

Inference

We used a delayed rejection adaptive Markov Chain Monte Carlo algorithm to fit models to the data (including replicates when available) using Bayesian inference[72,73]. For the one-step growth experiments, the priors were derived from the conventional estimates of the life history traits. The priors and likelihood functions were chosen to be either truncated normal or log-normal distributions. For the community experiments over multiple infection cycles, the traits of the one-step experiment fail the prior predictive check. A coordinate gradient descent algorithm was used to fit one of the replicates[74], which was used to inform priors, and the rest of the replicates were used to inform the likelihood in the Bayesian inference scheme. In all cases, posterior predictive checks and convergence tests were performed. Supplementary Information Section S1.5 provides a detailed description on inference methods.

Data availability

The datasets and code used for this project are available at: https://github.com/RaunakDey/VIMIMO_paper and are archived on Zenodo, https://doi.org/10.5281/zenodo.15314294.

Author contributions

MBS and JSW conceived the study. RD and ARC led theory and analyses with support from SJB, DD, DM, and JSW. NS led experiment design/implementation and data acquisition with support from ARC, CLS, MB, AM, and JG. CLS led sequencing and primer design. RD, ARC, and JSW wrote the manuscript with support from NS, DD, CLS, SJB, and MBS. RD and ARC generated tables and figures.

Acknowledgments

We thank Steven Wilhelm, Gary LeCleir, Naomi Gilbert, and Debbie Lindell for thoughtful feedback. We also thank members from the Weitz Group, Gabi Steinbach and Jessica Irons for administrative support and Tapan Goel for code review. We thank members of the Sullivan group Shaun Maxwell, Yueh-Fen Li, Guillermo Dominguez-Huerta, Lauren Chittick, and Siddharth Bhindwallam for help with preparing/sampling the synthetic community. The authors acknowledge the University of Maryland supercomputing resources (http://hpcc.umd.edu), Partnership for an Advanced Computing Environment (PACE) at the Georgia Institute of Technology, and Ohio Supercomputer Center made available for conducting the research reported in this paper. This work was supported by the National Science Foundation under Grant #1829636 (J.S.W.), Simons Foundation grant #72123 (J.S.W.), NSF EMERGE Biology Integration Institute award #2022070 (M.B.S.), and DOE Systems Biology award #DE-SC0023307 (M.B.S.). S.J.B. and J.S.W. are investigators at the University of Maryland-Institute for Health Computing, which is supported by funding from Montgomery County, Maryland and The University of Maryland Strategic Partnership: MPowering the State, a formal collaboration between the University of Maryland, College Park and the University of Maryland, Baltimore.

References

1. Chevallereau, A., Pons, B. J., van Houte, S. & Westra, E. R. Interactions between bacterial and phage communities in natural environments. *Nat. Rev. Microbiol.* **20**, 49–62 (2022).
2. Mirzaei, M. K. & Maurice, C. F. Ménage à trois in the human gut: interactions between host, bacteria and phages. *Nat. Rev. Microbiol.* **15**, 397–408 (2017).
3. Salmond, G. P. C. & Fineran, P. C. A century of the phage: past, present and future. *Nat. Rev. Microbiol.* **13**, 777–786, DOI: 10.1038/nrmicro3564 (2015).
4. Suttle, C. A. Marine viruses —major players in the global ecosystem. *Nat. Rev. Microbiol.* **5**, 801–812, DOI: 10.1038/nrmicro1750 (2007).
5. Rohwer, F. & Thurber, R. V. Viruses manipulate the marine environment. *Nature* **459**, 207–212, DOI: 10.1038/nature08060 (2009).
6. Weitz, J. S. & Wilhelm, S. W. Ocean viruses and their effects on microbial communities and biogeochemical cycles. *F1000 biology reports* **4**, 17–17, DOI: 10.3410/B4-17 (2012).
7. Flores, C. O., Meyer, J. R., Valverde, S., Farr, L. & Weitz, J. S. Statistical structure of host–phage interactions. *Proc. Natl. Acad. Sci.* **108**, E288, DOI: 10.1073/pnas.1101595108 (2011).
8. Flores, C. O., Valverde, S. & Weitz, J. S. Multi-scale structure and geographic drivers of cross-infection within marine bacteria and phages. *The ISME journal* **7**, 520–532, DOI: 10.1038/ismej.2012.135 (2013).
9. Weitz, J. S. *Quantitative Viral Ecology: Dynamics of Viruses and Their Microbial Hosts*. Monographs in Population Biology (Princeton Press, 2016).
10. Kauffman, K. M. *et al.* Resolving the structure of phage–bacteria interactions in the context of natural diversity. *Nat. communications* **13**, 372 (2022).
11. Breitbart, M., Bonnain, C., Malki, K. & Sawaya, N. A. Phage puppet masters of the marine microbial realm. *Nat. Microbiol.* **3**, 754–766, DOI: 10.1038/s41564-018-0166-y (2018).
12. Weitz, J. S. *et al.* Phage–bacteria infection networks. *Trends Microbiol.* **21**, 82–91, DOI: https://doi.org/10.1016/j.tim.2012.11.003 (2013).
13. Borin, J. M. *et al.* Rapid bacteria-phage coevolution drives the emergence of multiscale networks. *Science* **382**, 674–678 (2023).
14. Layeghifard, M., Hwang, D. M. & Guttman, D. S. Disentangling interactions in the microbiome: A network perspective. *Trends Microbiol.* **25**, 217–228, DOI: https://doi.org/10.1016/j.tim.2016.11.008 (2017).
15. Abedon, S. T. *Advances in Molecular and Cellular Microbiology* (Cambridge University Press, Cambridge, 2008).
16. Hyman, P. & Abedon, S. T. Practical methods for determining phage growth parameters. *Bacteriophages: methods protocols, volume 1: isolation, characterization, interactions* 175–202 (2009).
17. Dominguez-Mirazo, M., Harris, J. D., Demory, D. & Weitz, J. S. Accounting for cellular-level variation in lysis: implications for virus–host dynamics. *mBio* **0**, e01376–24, DOI: 10.1128/mbio.01376-24 (2024).
18. Nemergut, D. R. *et al.* Patterns and processes of microbial community assembly. *Microbiol. Mol. Biol. Rev.* **77**, 342–356 (2013).
19. Friedman, J., Higgins, L. M. & Gore, J. Community structure follows simple assembly rules in microbial microcosms. *Nat Ecol Evol* **1**, 109, DOI: 10.1038/s41559-017-0109 (2017).
20. Goldford, J. E. *et al.* Emergent simplicity in microbial community assembly. *Science* **361**, 469–474 (2018).
21. Ratzke, C., Barrere, J. & Gore, J. Strength of species interactions determines biodiversity and stability in microbial communities. *Nat. ecology & evolution* **4**, 376–383 (2020).
22. Grilli, J., Barabás, G., Michalska-Smith, M. J. & Allesina, S. Higher-order interactions stabilize dynamics in competitive network models. *Nature* **548**, 210–213 (2017).
23. Bairey, E., Kelsic, E. D. & Kishony, R. High-order species interactions shape ecosystem diversity. *Nat. communications* **7**, 12285 (2016).
24. Sanchez-Gorostiaga, A., Bajić, D., Osborne, M. L., Poyatos, J. F. & Sanchez, A. High-order interactions distort the functional landscape of microbial consortia. *PLoS Biol.* **17**, e3000550 (2019).

25. Chang, C.-Y., Bajić, D., Vila, J. C., Estrela, S. & Sanchez, A. Emergent coexistence in multispecies microbial communities. *Science* **381**, 343–348 (2023).

26. van den Berg, N. I. *et al.* Ecological modelling approaches for predicting emergent properties in microbial communities. *Nat. ecology & evolution* **6**, 855–865 (2022).

27. Chesson, P. Mechanisms of maintenance of species diversity. *Annu. review Ecol. Syst.* **31**, 343–366 (2000).

28. Ellner, S. P., Snyder, R. E., Adler, P. B. & Hooker, G. An expanded modern coexistence theory for empirical applications. *Ecol. letters* **22**, 3–18 (2019).

29. Lear, K. O., Whitney, N. M., Morris, J. J. & Gleiss, A. C. Temporal niche partitioning as a novel mechanism promoting co-existence of sympatric predators in marine systems. *Proc. Royal Soc. B* **288**, 20210816 (2021).

30. Rivett, D. W. & Bell, T. Abundance determines the functional role of bacterial phylotypes in complex communities. *Nat. microbiology* **3**, 767–772 (2018).

31. Tikhonov, M. Community-level cohesion without cooperation. *Elife* **5**, e15747 (2016).

32. Koskella, B. & Brockhurst, M. A. Bacteria–phage coevolution as a driver of ecological and evolutionary processes in microbial communities. *FEMS microbiology reviews* **38**, 916–931 (2014).

33. Fortuna, M. A. *et al.* Coevolutionary dynamics shape the structure of bacteria-phage infection networks. *Evolution* **73**, 1001–1011 (2019).

34. Blazanin, M. & Turner, P. E. Community context matters for bacteria-phage ecology and evolution. *The ISME J.* **15**, 3119–3128 (2021).

35. Holmfeldt, K. *et al.* Twelve previously unknown phage genera are ubiquitous in global oceans. *Proc. Natl. Acad. Sci.* **110**, 12798–12803 (2013).

36. Duhaime, M. B. *et al.* Comparative omics and trait analyses of marine Pseudoalteromonas phages advance the phage OTU concept. *Front. Microbiol.* **8**, 1241 (2017).

37. Deng, L. *et al.* Contrasting life strategies of viruses that infect photo- and heterotrophic bacteria, as revealed by viral tagging. *mBio* **3**, 10.1128/mbio.00373–12, DOI: 10.1128/mbio.00373-12 (2012). https://journals.asm.org/doi/pdf/10.1128/mbio.00373-12.

38. Dang, V. T., Howard-Varona, C., Schwenck, S. & Sullivan, M. B. Variably lytic infection dynamics of large *Bacteroidetes* podovirus phi38:1 against two *Cellulophaga baltica* host strains. *Environ. microbiology* **17**, 4659–4671 (2015).

39. Mayfield, M. M. & Stouffer, D. B. Higher-order interactions capture unexplained complexity in diverse communities. *Nat. ecology & evolution* **1**, 0062 (2017).

40. Billick, I. & Case, T. J. Higher order interactions in ecological communities: what are they and how can they be detected? *Ecology* **75**, 1529–1543 (1994).

41. Mickalide, H. & Kuehn, S. Higher-order interaction between species inhibits bacterial invasion of a phototroph-predator microbial community. *Cell systems* **9**, 521–533 (2019).

42. Datta, M. S., Sliwerska, E., Gore, J., Polz, M. F. & Cordero, O. X. Microbial interactions lead to rapid micro-scale successions on model marine particles. *Nat. communications* **7**, 11965 (2016).

43. Hu, J., Amor, D. R., Barbier, M., Bunin, G. & Gore, J. Emergent phases of ecological diversity and dynamics mapped in microcosms. *Science* **378**, 85–89 (2022).

44. Foster, K. R. & Bell, T. Competition, not cooperation, dominates interactions among culturable microbial species. *Curr. biology* **22**, 1845–1850 (2012).

45. Sanchez-Martinez, R. *et al.* Episomal virus maintenance enables bacterial population recovery from infection and promotes virus-bacterial coexistence. *The ISME J.* wraf066 (2025).

46. Schmitz, O. J., Buchkowski, R. W., Burghardt, K. T. & Donihue, C. M. Functional traits and trait-mediated interactions: connecting community-level interactions with ecosystem functioning. In *Advances in ecological research*, vol. 52, 319–343 (Elsevier, 2015).

47. Weitz, J. S., Hartman, H. & Levin, S. A. Coevolutionary arms races between bacteria and bacteriophage. *Proc. Natl. Acad. Sci.* **102**, 9535–9540 (2005).

48. Seed, K. D. Battling phages: how bacteria defend against viral attack. *PLoS pathogens* **11**, e1004847 (2015).

49. Labrie, S. J., Samson, J. E. & Moineau, S. Bacteriophage resistance mechanisms. *Nat. Rev. Microbiol.* **8**, 317–327 (2010).

50. Abedon, S. T., Herschler, T. D. & Stopar, D. Bacteriophage latent-period evolution as a response to resource availability. *Appl. environmental microbiology* **67**, 4233–4241 (2001).

51. Nabergoj, D., Modic, P. & Podgornik, A. Effect of bacterial growth rate on bacteriophage population growth rate. *MicrobiologyOpen* **7**, e00558 (2018).

52. Talmy, D. *et al.* Contrasting controls on microzooplankton grazing and viral infection of microbial prey. *Front. Mar. Sci.* **6**, 182 (2019).

53. Dennehy, J. J. & Wang, I.-N. Factors influencing lysis time stochasticity in bacteriophage λ. *BMC microbiology* **11**, 1–12 (2011).

54. Wedd, C. *et al.* Single-cell imaging of the lytic phage life cycle in bacteria. *bioRxiv* 2024–04 (2024).

55. Baker, C. W. *et al.* Genetically determined variation in lysis time variance in the bacteriophage φx174. *G3: Genes, Genomes, Genet.* **6**, 939–955 (2016).

56. Hinson, A. *et al.* A model of algal-virus population dynamics reveals underlying controls on material transfer. *Limnol. Oceanogr.* **68**, 165–180 (2023).

57. Seth, E. C. & Taga, M. E. Nutrient cross-feeding in the microbial world. *Front. Microbiol.* **5**, 350, DOI: 10.3389/fmicb.2014.00350 (2014).

58. Pande, S. *et al.* Fitness and stability of obligate cross-feeding interactions that emerge upon gene loss in bacteria. *The ISME J.* **8**, 953–962, DOI: 10.1038/ismej.2013.211 (2014).

59. Lindell, D. *et al.* Genome-wide expression dynamics of a marine virus and host reveal features of co-evolution. *Nature* **449**, 83–86 (2007).

60. Howard-Varona, C. *et al.* Environment-specific virocell metabolic reprogramming. *The ISME J.* **18**, wrae055 (2024).

61. Bondy-Denomy, J. *et al.* Prophages mediate defense against phage infection through diverse mechanisms. *The ISME journal* **10**, 2854–2866, DOI: 10.1038/ismej.2016.79 (2016).

62. Mavrich, T. N. *et al.* Evolution of superinfection immunity in cluster a mycobacteriophages. *mBio* **10**, e00971–19, DOI: 10.1128/mBio.00971-19 (2021).

63. Berngruber, T. W., Weissing, F. J. & Gandon, S. Inhibition of superinfection and the evolution of viral latency. *J. Virol.* **84**, 10200–10208, DOI: 10.1128/JVI.00865-10 (2010).

64. Geesink, P., Ter Horst, J. & Ettema, T. J. More than the sum of its parts: uncovering emerging effects of microbial interactions in complex communities. *FEMS Microbiol. Ecol.* fiae029 (2024).

65. Alseth, E. O. *et al.* The impact of phage and phage resistance on microbial community dynamics. *PLOS Biol.* **22**, 1–25, DOI: 10.1371/journal.pbio.3002346 (2024).

66. Castledine, M. & Buckling, A. Critically evaluating the relative importance of phage in shaping microbial community composition. *Trends Microbiol.* (2024).

67. Holmfeldt, K., Middelboe, M., Nybroe, O. & Riemann, L. Large variabilities in host strain susceptibility and phage host range govern interactions between lytic marine phages and their *Flavobacterium* hosts. *Appl. Environ. Microbiol.* **73**, 6730–6739, DOI: 10.1128/AEM.01399-07 (2007).

68. Wichels, A. *et al.* Bacteriophage diversity in the North Sea. *Appl. Environ. Microbiol.* **64**, 4128–4133, DOI: 10.1128/AEM.64.11.4128-4133.1998 (1998).

69. Melissa, D., Antje, W. & Matthew, S. Six *Pseudoalteromonas* strains isolated from surface waters of Kabeltonne, Offshore Helgoland, North Sea. *Genome Announc.* **4**, e01697–15, DOI: 10.1128/genomeA.01697-15 (2016).

70. Shampine, L. F. & Reichelt, M. W. The MATLAB ODE suite. *SIAM journal on scientific computing* **18**, 1–22 (1997).

71. Hurtado, P. J. & Kirosingh, A. S. Generalizations of the 'Linear Chain Trick': incorporating more flexible dwell time distributions into mean field ode models. *J. Math. Biol.* **79**, 1831–1883, DOI: 10.1007/s00285-019-01412-w (2019).

72. Haario, H., Saksman, E. & Tamminen, J. An adaptive metropolis algorithm. *Bernoulli* 223–242 (2001).

73. Haario, H., Laine, M., Mira, A. & Saksman, E. DRAM: efficient adaptive MCMC. *Stat. computing* **16**, 339–354 (2006).

74. Wright, S. J. Coordinate descent algorithms. *Math. programming* **151**, 3–34 (2015).

75. Haario, H., Laine, M., Mira, A. & Saksman, E. Dram: Efficient adaptive mcmc. *Stat. Comput.* **16**, 339–354, DOI: 10.1007/s11222-006-9438-0 (2006).

76. Gelman, A. & Rubin, D. B. Inference from iterative simulation using multiple sequences. *Stat. science* **7**, 457–472 (1992).

77. Vats, D. & Knudson, C. Revisiting the gelman–rubin diagnostic. *Stat. Sci.* **36**, 518–529 (2021).

78. Geweke, J. Evaluating the accuracy of sampling-based approaches to the calculation of posterior moments. Tech. Rep., Federal Reserve Bank of Minneapolis (1991).